


Scale-up of Microfiltration Processes

Susanne Haindl^{1,2,*}, Julia Stark¹, Jannik Dippel^{1,2}, Sebastian Handt¹, and Annette Reiche¹

DOI: 10.1002/cite.201900025

 This is an open access article under the terms of the Creative Commons Attribution License, which permits use, distribution and reproduction in any medium, provided the original work is properly cited.



Supporting Information
available online

A flow rate and resistance-based approach for upscaling of microfiltration processes from lab scale to process scale is presented, in correlation with biopharmaceutical processes. Basic element is the modeling of filtration curves using a resistance-in-series model based on the Darcy equation. The influences of the filtration setup and the fouling layer are described as additional resistances that change in course of filtration. The necessary parameters, such as setup resistances and filtration areas, are determined by water flow rate measurements. The model is validated by filtration of a particulate test solution. The presented approach can be used for constant flow and constant pressure driven filtration processes.

Keywords: Biopharmaceutical process, Microfiltration, Scale-up

Received: January 30, 2019; *revised:* January 17, 2020; *accepted:* January 28, 2020

1 Microfiltration in Biopharmaceutical Process Design

1.1 Typical Aspects of Biopharmaceutical Processing

Biopharmaceuticals (proteins and derivatives, parts of DNA and hormones [1]) are usually produced by cell culture processes. The manufacturing process of therapeutic proteins can be separated in an upstream part, comprising the cell culture process and the harvest, and in a downstream part, the purification of the target protein and formulation of a protein drug [2]. The manufacturing process is concluded by fill & finish, the final sterile filtration and the filling of a protein drug [3]. An overview of the bioprocess is shown in Fig. 1.

Every biopharmaceutical process contains various filtration steps [7]. Product media, buffer and cell culture media have to be sterile filtered [8,9]. Main filtration steps are depth filtration, bioburden reduction and sterile filtration, virus filtration, ultra- and diafiltration [5, 10, 11].

There is a general trend towards single-use equipment in biopharmaceutical production. Consequently, filtration equipment is single use as well, using filter capsules, which can be easily handled and do not need cleaning in contrast to a multi-use filter housing [12]. A review on the subject of membrane modules for process scale is published by van Reis [9]. An example for single-use devices are T-Style MaxiCaps[®] by Sartorius Stedim Biotech, which were used in this study and are described in Sect. 2.2.1. Filtration equipment contains usually 10³–30³ capsules depending on the batch size. Filter capsules are often used as a component

of a ready to use preconfigured system. Only the tubing has to be connected before use. Capsules contain pleated single or double-layer membranes, encompassed by non-wovens, with filtration areas usually between 0.6 and 1.1 m², for 10³ [9, 13, 14].

Biopharmaceutical media are chemically seen suspensions or colloidal solutions. Product and central component of formulation are proteins, which are dispersed nanoparticles in aqueous solution. Further formulation components are dissolved molecules like buffer, electrolytes, sugar, surfactants, etc. [15, 16]. Viscosity can vary between 1 cP for diluted systems and 50 cP for full therapeutic formulations in final fill filtration. The viscosity of the formulation has impact on the filtration flow across the filter. High-concentrated protein solutions are fluids with non-Newtonian behavior and show shear thinning behavior [17]. Composition, pH and viscosity of product formulation change in course of the biopharmaceutical process, resulting in a different degree of filter fouling [18, 19]. Filter fouling is usually not an issue for diluted solutions but a severe problem for clarification filtration, filtration of bulk drug substance

¹Susanne Haindl, Julia Stark, Jannik Dippel, Sebastian Handt, Annette Reiche
susanne.haindl@sartorius.com
Sartorius Stedim Biotech GmbH, August-Spindler-Straße 11, 37079 Göttingen, Germany.

²Susanne Haindl, Jannik Dippel
Gottfried-Wilhelm-Leibniz Universität Hannover, Institut für Technische Chemie, Callinstraße 5, 30167 Hannover, Germany.

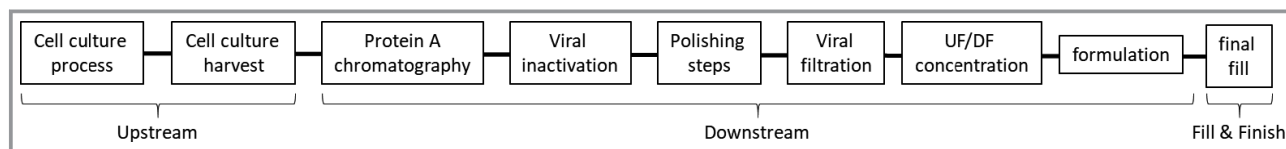


Figure 1. Schematic overview of a bioprocess for manufacturing of monoclonal antibodies [4–6].

and final fill filtration, depending on concentration of solution, particle load and process conditions [7, 20, 21].

Most biopharmaceutical filtration steps are constant flow driven [22, 23]. This mode of operation fits perfectly in the general biopharmaceutical process flow [7]. Filter fouling is usually lower for constant flow operation [24].

Main process parameters for filter devices are flow rate and transmembrane pressure. Their relationship during filtration of a fluid through a membrane filter can be described by the Darcy equation (see Eq. (6), Sect. 2.1) independent of the mode of operation.

For biopharmaceutical process design, the overall process has to be considered, not just an isolated filtration step. A filtration process is always part of a sequential arrangement, which determines the necessary process parameters. Flow rates for example have to be high enough to keep up with filling machines [25], to provide buffer for column chromatography, or to evade enzymatic degradation [26]. Furthermore, it is well known that process conditions have impact on filter fouling or product quality. A high flow rate can cause protein aggregation due to shear stress [18]. A very low flow rate can increase filter fouling due to a long interaction time between protein and membrane surface [18].

Biopharmaceutical process engineering shall ensure maximum product yield and process consistency by choice of operation conditions and equipment. The food and drug administration (FDA) has strengthened regulatory measures to improve biopharmaceutical process consistency. Filtration steps play an important role for the proper removal of microorganisms and particular contaminants, and by this have an essential impact on the smooth progress of the whole biopharmaceutical process, the product yield and quality [7, 8, 27]. Since the biopharmaceutical formulations are quite expensive, filtration equipment should be properly sized to avoid dead volume.

1.2 Current Upscaling Procedure for Dead-End Microfiltration

Scale-up is an engineering approach in process filtration for selection of suitable process filtration equipment, filter sizing, and process parameters, i.e., the estimation of the necessary filter area or the filter capacity for filtration of a given fluid volume for a specified set of operating conditions.

Experimentally, the filter capacity for filtration of a given fluid phase is determined by small-scale filtration trials with the area A_{test} , usually on the basis of constant pressure fil-

tration trials [28]. For these small-scale experiments, scaling devices with a minimal membrane area are available, such as Sartoscale 25 by Sartorius Stedim Biotech GmbH [29], Optiscales[®] by Merck KGaA [28] or the Mini Kleenpak[™] products by Pall Corporation [30].

In small scale, direct measurement of flow rate is often not possible with the necessary accuracy. Alternatively, the filtered mass can be collected by a balance and the flow rate can be calculated by the first derivative of the volume with respect to time. Currently, discussion of filtration processes and filter fouling are quite frequently based on the filtered volume versus time plot.

In literature, scale-up experiments are performed by determination of the filter capacity. The filter capacity is defined by the V_{final} value, which is the maximum reached filtrate volume required for complete filter blocking. In a lab-scale trial pressure, filtrate volume and time are recorded. Resulting experimental data are displayed in a volume vs. time plot.

The necessary membrane area A_{batch} for filtration of a batch size of the volume V_{batch} can be calculated by the following equation using V_{final} and A_{test} :

$$A_{\text{batch}} = SF \frac{V_{\text{batch}}}{V_{\text{final}}} A_{\text{test}} \quad (1)$$

Usually the risk of underestimating the filter area is minimized by introducing a safety factor, SF . The safety factor is necessary to compensate the variability usually connected with upscaling processes; e.g., industrial membranes show a variability of performance and filtration devices might vary concerning geometric dimensions. This may be the case for very small scaling devices with filter area of few square centimeters. Additionally, there is a big range of possible process conditions for filtration [21, 31]. Safety factors are given with values of 0.75–0.9 [32], 1.1–2.5 [33], 1.3–2 [34], 1.5 [9] or 2 [24], in dependence of the process (constant flow or constant pressure) [32, 35] or of the blocking mechanism of the filtration [32]. The importance of safety factors for biopharmaceutical process development is reported by Lutz et al. [33].

Customers in the biopharmaceutical industry usually require upscaling trials with a minimum amount of the formulation, as the respective formulations are quite expensive and thermodynamically not stable. Therefore, small-scale trials must be reliable, because they are used to evaluate the impact on product quality and the basics for the large-scale filtration process. To minimize the amount of necessary scaling experiments, first the basic aspects of a filtration

process have to be evaluated (batch volume, process time, necessary filtration flow). Mathematic modeling of the filtration process helps to minimize experimental efforts, and with that to reduce volume of filtration media required for test trials.

For upscaling it has to be considered that biopharmaceutical formulations usually show process-dependent filter fouling. Therefore, the small-scale trials should be performed in the same mode as the process trials, usually with a constant flow rate.

The filter capacity V_{final} can be extrapolated by fitting a pore blocking model to the experimental filtration data [36]. Modeling of filter fouling on the basis of pore blocking models has a history in filtration technology that began in the 1930s. Usually four blocking models are used for description of filter fouling: complete blocking, standard blocking, intermediate blocking, and cake filtration. The general blocking law for all four cases is:

$$\frac{d^2t}{dV^2} = k \left(\frac{dt}{dV} \right)^n \quad (2)$$

The blocking index n varies with values between 0 and 2 in dependence on the fouling mechanism. Theoretical background and calculation basis are described in a review article by Iritani et al. [36]. The blocking models were developed for ideal fluids with a narrow particle size distribution flowing through ideal membranes with cylindrical pores. Neither membranes nor fluids fulfill these model requirements in industrial process filtration. Microfilter membranes exhibit a sponge-like porous structure rather than cylindrical pores [9, 36]. Most industrial process media, especially biopharmaceutical formulations, are colloidal solutions with limited thermodynamic stability as described above [15, 16, 37]. Dispersed particles are not necessarily spherical and undergo interactions between each other and with the membrane surface. Moreover, the blocking mechanism can change during filtration, e.g. at the beginning small particles deposit within the membrane pores until the pores are so tight, they get plugged by a particle. Therefore, the predictability of the use of single blocking models for upscaling and filter sizing is limited and upscaling results based on those models deviate significantly [32, 35, 38]. The predictability can be slightly improved by combining several blocking models. The combination of blocking models extends the number of parameters that can be modified, resulting in generated data closer to experimental measurements [39, 40].

An example of the mentioned approach for upscaling of filtration processes, set of experiments and working methods behind is given by Rajniak et al. [32] for the redundant sterilizing filtration of an active pharmaceutical ingredient solution using a PVDF membrane filter with scaling from a 47-mm filter disc to pilot and production scale. Different blocking models and combinations were applied for curve fitting. The calculated values usually underestimated the

experimentally determined capacity values and were consequently regarded as worst-case scenario. An extra safety factor of 2 was included due to large batch-to-batch variation. Furthermore, the article gives an overview about resistances of filtration equipment in dependence on scale and details of construction. Finally, it was stated that sterilizing filtration is not a linearly scalable unit operation due to the fact that the pressure-normalized initial flux is different for the scaling devices used. The initial flux decreases with increasing filter area due to occurrence of additional flow resistances connected with device construction, tubing and fittings [32]. Other reviews about experimental procedure, theoretical approaches, and aspects to consider for conducting microfiltration upscaling studies are given in the literature [31, 32, 34, 41].

To improve the predictability and to avoid the use of blocking laws, it is generally recommended to do calculations based on small-scale filtration trials run until nearly complete membrane blocking. In case of limited amount of test solution this is a problem.

There is a strong trend in recent literature to use flow rate and resistance to monitor filtration processes and filter fouling [36]. The resistance can be calculated by the Darcy equation (Sect. 2.1). The viscosity of a filtration fluid is the only value required for the calculation of the membrane resistance on top of the parameter set encompassing the filtration time, flux (or volume) and differential pressure. The approach has many advantages: Monitoring of flow rate and resistance vs. throughput (filtrate volume per effective membrane area) connects both change of flow rate and the occurrence of fouling processes with the passage of contaminants through the filter. Moreover, it gives insight in the process dependency of filter fouling, which is quite strong for biopharmaceutical process filtration. The change of the initial water flux with device size can be visualized. The magnitude of the resistance of the membrane and the filter housing can be quantified, which allows to identify experimental issues, e.g., reduction of effective filter area by insufficient wetting or inclusion of air within a system.

1.3 Aim of this Work

This work presents a flow rate and resistance-in-series based model for upscaling of filtration processes, which does not require knowledge of blocking mechanism. In the following the approach for this model is described beginning with the chapter model development, which contains the necessary theoretical background for the description of flow rate and resistance (Sect. 2.1), information about the experimental setups and filter devices (Sect. 2.2), and their flow properties (Sect. 2.3). Sect. 2.4 explains how filter devices can be described by a resistance-in-series model, based on the Darcy-equation, and how the device resistance and effective filter area can be determined by water flow measurements.

Filtration trials are performed and described in Sect. 2.5 in order to show how the formation of the fouling layer can be visualized by calculation of the filtration flux or the resistance versus throughput curves. Basic equations for modeling of filtration curves for target filtration conditions and devices on the basis of small-scale filtration trials are summarized in Sect. 2.6 for constant pressure filtration processes and in Sect. 2.7 for constant flow filtration processes.

Finally, case studies are described to validate the scale-up approach and the calculation basis. Data are summarized in the chapter model validation with a constant pressure filtration upscaling example (Sect. 3.1) and a constant flow downscaling example (Sect. 3.2).

2 Model Development

2.1 Flow Rate and Resistance in Microfiltration – General Aspects

For evaluation of filtration experiments, volume V , differential pressure ΔP and the corresponding time t are monitored. The volume V , normed by the effective filtration area A_{mem} , is here defined as throughput \tilde{V} .

$$\tilde{V} = \frac{V}{A_{\text{mem}}} \quad (3)$$

With the filtration volume V , water flow rate J can be calculated.

$$J = \frac{dV}{dt} \quad (4)$$

The filtration flux J° can be defined as the normed water flow rate J , using the effective filtration area A_{mem} :

$$J^\circ = \frac{J}{A_{\text{mem}}} \quad (5)$$

The flow rate of a fluid through a porous membrane filter can be described with the Darcy equation, which is usually written in the following form for filtration:

$$J = \frac{\Delta p A_{\text{mem}}}{\eta R^\circ} \quad (6)$$

The flow rate J depends on the filtration process parameter Δp , the fluid viscosity η , and the membrane properties (resistance R° and membrane area A_{mem}).

Darcy's law is an empirical equation, which was later explained as a simplified solution of the Navier-Stokes equation. The Darcy equation is valid for laminar flow, hence, can be applied in case of low Reynolds numbers [42]. The Reynolds number Re is the ratio of inertia forces to the viscous forces. Within a straight tube Re is a function

of filtration flux J° , density ρ , the inner tube diameter d_i , and solution viscosity η .

$$Re = \frac{J^\circ \rho d_i}{\eta} \quad (7)$$

Knowing the Reynolds number is important for the estimation of flow properties, whether fluid flow is laminar or turbulent. The critical Reynolds number in a straight tube is $Re = 2320$. Below that value, fluid flow is laminar. Between $2320 < Re < 8000$ both laminar and turbulent fluid flow can occur, above $Re = 8000$ fluid flow is turbulent [43]. A turbulent flow rate causes additional resistances in the system. Hence, the device resistance depends on the flow rate and can be determined for a given filter device by measurement of water flow rate versus differential pressure.

As a result of Navier-Stokes, fluid flow resistances can be calculated the same way as in electrical circuits. Resistances in series can be summed up as demonstrated in Eq. (8).

$$R_{\text{ges}} = \sum_i R_i \quad (8)$$

The reciprocal value of resistances connected in parallel setup add up to the reciprocal value of the total resistance of the setup (Eq. (9)).

$$\frac{1}{R_{\text{ges}}} = \sum_i \frac{1}{R_i} \quad (9)$$

Furthermore, the resistance of a module can be calculated in terms of the resistances of the single components that have a perceptible contribution [24, 31, 44, 45]. Here this approach will be applied to filter devices. Fig. 2 outlines the resistances of a device that impact on filtration flow rate. As the resistance are in series here, they have to be added up. For a large process, the resistance of the setup depends not only on the membrane and device design but also on all the technical equipment, e.g., fittings, tubes or pressure gauges [32, 33]. Filter fouling contributes to the membrane resistance and leads to an increase in pressure for constant flow operations or to a decrease in flow rate for constant pressure filtrations as well.

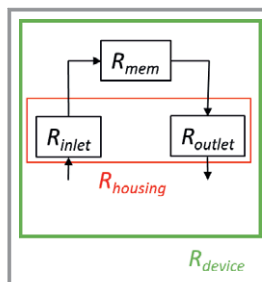


Figure 2. Components contributing to the resistance of a filtration device; $R_{\text{device}} = R_{\text{mem}} + R_{\text{housing}}$.

2.2 Experimental Approach

For the experiments described in this paper, various filter devices and filter discs were used for water flow rate measurements and filtration trials as summarized in Tab. 1. A particulate test media (0.1 wt % mixture of Caro Kaffee and Ovomaltine) has been used for the filtration trials with a viscosity of 1 mPa s and a broad particle size distribution with a diameter between 0.1 and 10 μm . Measurements are performed in triplicates. All housings for filter discs use a steel grid by Haver & Boecker as membrane support.

2.2.1 Design of T-Style MaxiCaps[®]

An example for single-use devices used in process filtration are T-Style MaxiCaps[®] by Sartorius Stedim Biotech GmbH. T-Style MaxiCaps[®] filter devices with 0.6 m², 1.2 m² and 1.8 m² embedded membrane area are available, with different connector styles and with membranes of different pore size (Tab. 1). Therefore, they are a good basis for examination of water flow data. Blueprints of T-Style MaxiCaps[®] and of the different connector styles are presented in the Supporting Information. For connector styles always two letters are given, the first one for the inlet, the second one for the outlet. In this work, only devices with the same inlet and outlet are considered: “O” (1/2” single stepped hose barb), “S” (1 1/2” Tri-Clamp), and “Y” (1” single stepped hose barb) [46]. All MaxiCaps[®] are made of the same 10” building blocks containing 0.6 m² membrane area. For fabrication of 20” or 30” MaxiCaps[®] those 10” building blocks are combined by stacking.

Scaling trials were performed with membrane material from the Sartopore[®] 2 product family, which contain membranes based on polyether sulfone (PES). A double-layer membrane sandwich is used with a prefilter/main filter combination of 0.45/0.2 μm pore size, or a combination of 0.2/0.1 μm pore size.

2.3 Estimation of Flow Properties

The Reynolds number is estimated for fluid flow through the membrane pores and through the connectors of the devices according to Eq. (7). For the membrane material a water flow rate of 21 mL min⁻¹ cm⁻² (Δ 12600 L h⁻¹ m⁻²) was measured for Sartopore[®] 2 main filter membrane with a nominal pore size of 0.2 μm and flow rate within a pore is assumed to be the same as flow rate over the whole filter disc. Applying this to Eq. (7), a Reynolds number $Re \ll 1$ is obtained. Flow rate through the membrane pores under common filtration conditions can be assumed to be laminar.

The Reynolds number of a membrane housing depends only on the inlet and the outlet of T-Style MaxiCaps[®]. This value can be estimated by the inner diameter. For “S”-connectors and “Y”-connectors, the inner diameter is 19 mm, and for “O”-connectors 8.8 mm. For devices with 0.6 m² membrane area, 132 L min⁻¹ water should be able to pass the device at 1 bar if the complete membrane area is used and no additional device resistance exists. For the “S”-connectors this equals to a Reynolds number of $1.5 \cdot 10^6$. This estimation indicates that turbulent flow occurs through the connectors of the devices. As a consequence, there is a pressure loss that is not related to the membrane.

2.4 Resistance and Effective Filtration Area of T-Style MaxiCaps[®] by Water Flow Rate Measurements

Measurement data of water flow rates for T-Style MaxiCaps[®] are presented in Fig. 3a for 0.1 μm pore size and in Fig. 3b for 0.2 μm pore size. For this study T-Style MaxiCaps[®] with different membrane areas and devices with different connectors were chosen. The water flow rates that

Table 1. Overview of performed filtration experiments, membrane areas, connectors and setups used in this paper. For filtration devices embedded area according to product specification sheet is given [13].

Device	Setup	Embedded membrane area [cm ²]	Process mode	Medium	Housing / connectors
25-mm filter discs	1	2.75	constant flow	particulate solution	stainless-steel filter housing
47-mm filter discs	2	14.1	constant pressure	particulate solution	stainless-steel filter housing
142-mm filter discs	2	136	constant pressure	particulate solution	stainless-steel filter housing
Size 4 capsules	2	150	constant pressure	particulate solution	(3/4”) triclamp
T-Style MaxiCaps [®]	3	10” capsule: 6000 20” capsule: 12 000 30” capsule: 18 000	constant pressure	water	S = 1 1/2” triclamp (inner diameter of 19 mm) O = 1/2” single stepped hose barb (inner diameter of 8.8 mm) Y = 1” single stepped hose barb (inner diameter of 19 mm)

can be expected according to Darcy's law are included as well.

Fig. 3 shows a nonlinear dependency between water flow rate and pressure of the T-Style MaxiCaps[®] measured. Water flow rate increases with increasing pressure as expected, but less than estimated with the Darcy equation. Connectors have a significant impact on water flow rate at higher differential pressures if they are undersized. "O"-connectors (data in black) are more limiting to flow rate than "Y"- or "S"-connectors (data in green and red). Furthermore, the data of "O"-connectors indicate that inlet and outlet have the most limiting effect on the water flow rate.

Devices with membranes with a nominal pore size of 0.2 μm (Fig. 3b) show a higher water flow rate than devices with a membrane with nominal pore size of 0.1 μm (Fig. 3a) due to the lower membrane resistance. This trend is clearly obvious for devices with "S"- and "Y"-connectors. For devices with "O"-connectors hardly any difference can be seen between different membrane areas or pore sizes.

Doubling or triplicating membrane area (by using 1.2 m² or 1.8 m² compared to 0.6 m²) does not have a linear effect on water flow rate data as can be seen in Fig. 3. Instead the water flow rate data are clearly lower than expected. These results can be explained by calculation of the resistance of

each device. Fig. 4 summarizes total device resistances, R_{tot}° in dependence on water flow rate for the data of T-Style MaxiCaps[®] presented in Fig. 3. Resistances of T-Style MaxiCaps[®] were calculated according to Darcy's law (Eq. (6)). A linear relationship between device resistance R_{tot}° and water flow rate J can be observed.

In a next step, the membrane and the device resistance are calculated. As discussed in Sect. 2.3, Reynolds numbers for fluid flow through membrane pores suggest laminar fluid flow, and Reynolds numbers through connectors of MaxiCaps[®] indicate turbulent flow. Therefore, for each device, a linear regression is applied to the $R_{tot}^{\circ}(J)$ data (Fig. 4) and the intercept taken as membrane resistance R_{mem}° . For calculation of the housing resistance according to Eq. (8) the membrane resistance is subtracted from the total device resistance, Eq. (11) is obtained. Additionally, the resistances are examined with regard to each device, so the membrane area is not included in the Darcy equation here (Eq. (10)). Because of this, the dimension of the resistance changes to m⁻³.

$$R = \frac{p}{\eta J} \quad (10)$$

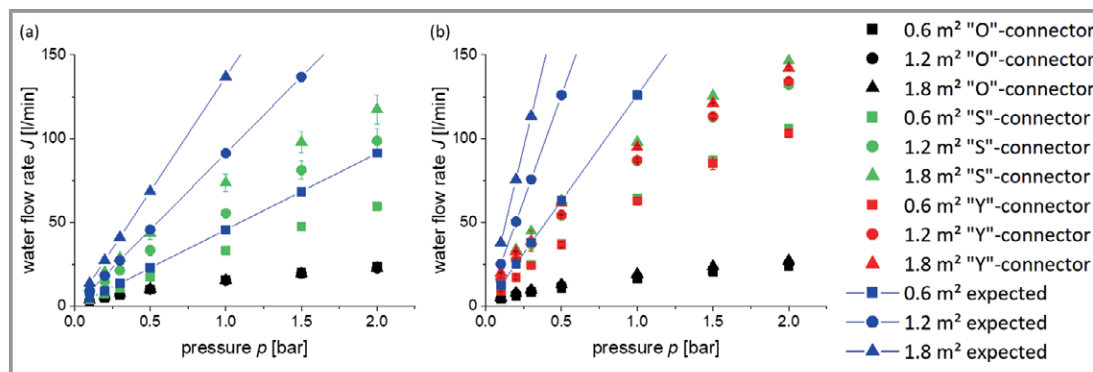


Figure 3. Water flow rate data of T-Style MaxiCaps[®] of Sartopore[®] 2 for 0.1 μm pore size (a) and 0.2 μm pore size (b). Measurement data and expected data according to Darcy's law for different connector styles and membrane areas.

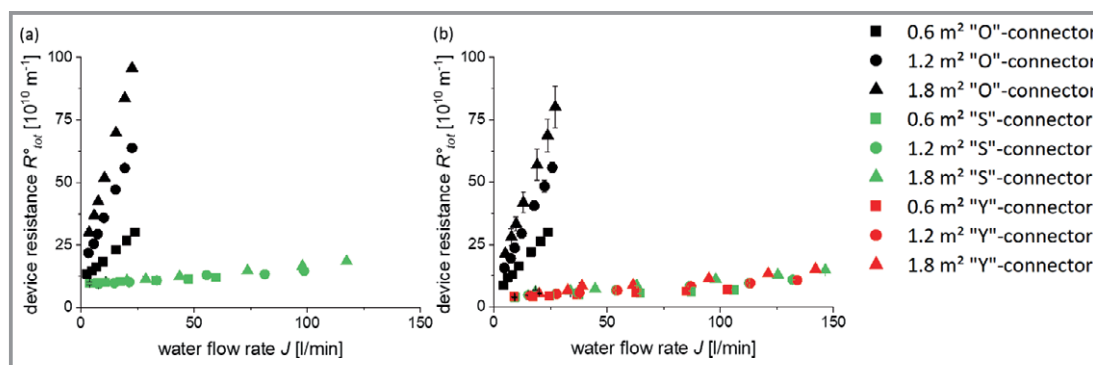


Figure 4. Device resistance (R_{tot}°) data of T-Style MaxiCaps[®] for 0.1 μm (a) and 0.2 μm (b) pore size, different connectors and different membrane areas.

The housing resistance R_{housing} is calculated by omitting the membrane resistance R_{mem} from the device resistance R_{tot} as shown in Eq. (11):

$$R_{\text{housing}} = R_{\text{tot}} - R_{\text{mem}} = R_{\text{tot}} - \frac{R_{\text{mem}}^{\circ}}{A_{\text{mem}}} \quad (11)$$

Resistances that consider the influence of the respective cross-section area are marked by a circle. The correlation between membrane resistance R_{mem} and specific membrane resistance R_{mem}° is calculated with the following equation:

$$R_{\text{mem}}^{\circ} = R_{\text{mem}} A_{\text{mem}} \quad (12)$$

Here A_{mem} is the effective membrane area that contributes to filtration flow rate within a device. The effective membrane area A_{mem} might be lower than the embedded or geometrically determined membrane area for constructive filter design. This is especially the case for larger pleated filter products with complex flow design. As a consequence, it can be said for the filter discs that the geometrically measured membrane area is the effective membrane area; for the pleated filter devices the effective membrane area is smaller than the embedded membrane area and should be measured by H_2O flow rate measurements.

Calculated housing resistances R_{housing} according to Eq. (11) are shown in Fig. 5 in dependence on water flow rate. In Figs. 5a and 5b a line for the "O"-connectors and another for the "S"- and "Y"-connectors can be observed, independent of the filtration area and the membrane pore size. For each connector (regardless of the membrane pore size), a linear function is fitted to the data. As the intercept has been taken out as the membrane resistance R_{mem} , they can be described by just one constant k_i , the slope of the line. For "O"-connectors, that value is $k_{\text{O}} = 1.56 \pm 0.04 \cdot 10^{13} \text{ min m}^{-6}$, for "S"- and "Y"-connectors k_{S} and k_{Y} are $0.041 \pm 0.001 \cdot 10^{13} \text{ min m}^{-6}$. Therefore, the housing resistance can be described by a function of filtration flow rate:

$$R_{\text{housing}}(J) = k_i J \quad (13)$$

The intercept in Fig. 4 can be used to calculate the effective membrane area A_{mem} . If the specific membrane resistance R_{mem}° is precisely known (e.g., due to water flow measurements of a filter disc), that value can be compared to the measured membrane resistance, R_{mem} to determine the effective membrane area A_{mem} via Eq. (12).

The housing resistances R_{housing} calculated according to Eq. (13) and the effective membrane area A_{mem} are the two main parameters for the scale-up calculations presented in the following chapters.

2.5 Small-Scale Filtration Experiments for Measurement and Description of Filter Fouling

For scale-up experiments the model solution described in Sect. 2.2 is used. Filtration experiments are performed with filter discs of Sartopore[®] 2 (14.1 cm² effective membrane area and 136 cm² effective membrane area, which is equal to the geometrically determined membrane area given in Tab. 1). Filter areas have been measured after filtration, as the test solution dyes the membrane. Filtration is performed by constant pressures of 0.5 and 1 bar. The measurement results are presented in Fig. 6.

According to the usual industrial practice, filtration data are presented in a volume vs. time plot as presented in Fig. 6a. Filtration flux and the resistances were calculated according to Eqs. (5) and (6) and plotted versus filtration time and throughput. The results are presented in Fig. 6b–e. Presentation of data as demonstrated in Fig. 6 allows to visualize many effects connected with filtration and filter fouling:

- differences of the initial flux caused by a change of process conditions or different device resistances (Fig. 6b and 6d)
- a decrease of filtration time until complete membrane blocking in case of filtration at higher pressure due to increasing flow (Fig. 6b)
- it can be shown whether process conditions have an impact on filter fouling. Resistance vs. throughput curves, shown in Fig. 6e are identical. They would deviate if

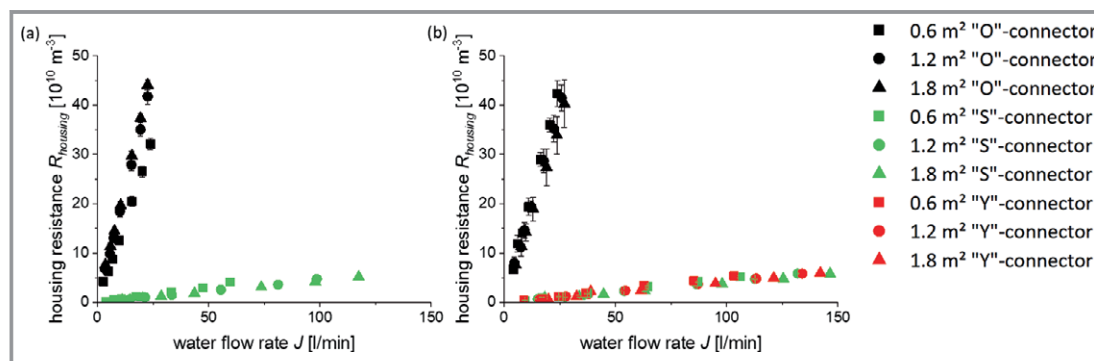


Figure 5. Resistance data of device housing of T-Style MaxiCaps[®] for 0.1 μm (a) and 0.2 μm (b) pore size, different membrane areas and different connectors.

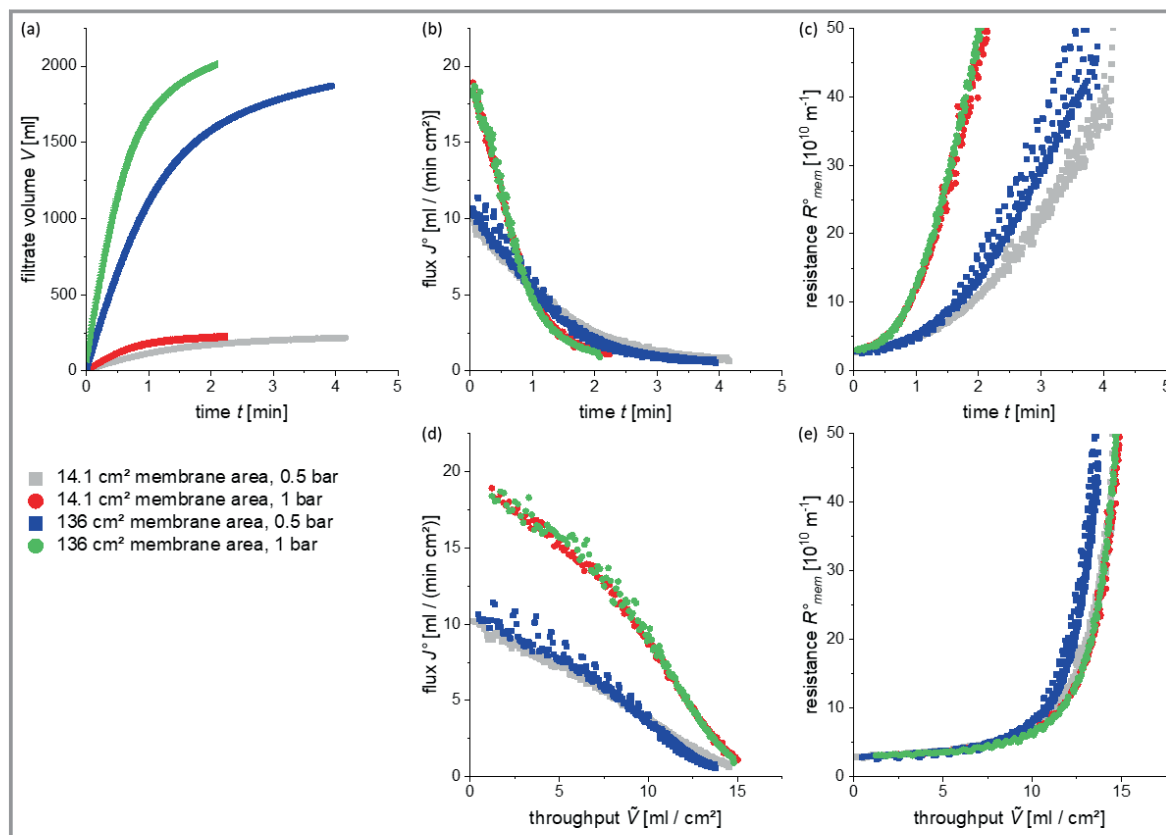


Figure 6. Results of filtration experiments with model solution for two different transmembrane pressures and two effective membrane areas. a) Measured filtration curve, b) calculated filtration flow vs. time, c) calculated area specific resistance vs. time, d) and e) the respective data vs. throughput.

filtration process conditions had an impact on filter fouling.

- different resistances of filtration devices are indicated by different initial values of the resistance versus time or throughput plots (Figs. 6c and 6e, here device resistances are equal).

Filter fouling is caused by a separation process. The transport rate of particles is directly proportional to the filtration flow rate. However, some biopharmaceutical fluid phases, e.g., protein formulations, can be easily destabilized during filtration. Colloidal solutions always show a limited thermodynamic stability, shear stress can cause protein aggregation, and adsorption phenomena can be enhanced by long residence time of protein near the membrane surface. All these side reactions lead to additional fouling and can be influenced by filtration flow rate.

The impact of process conditions on the fouling rate can be visualized in the resistance vs. throughput plot for constant pressure as well as constant flow driven filtration processes.

Upscaling calculations in Section 2.6 and 2.7 are based on the fact that filter fouling, which occurs in course of filtration, leads to formation of an additional resistance for the fouling layer, as can be observed by the increase of mem-

brane resistance in dependence of throughput in course of filtration (Fig. 6e).

The cause of the increase in membrane resistance or the mechanism of filter fouling is not important for the upscaling approach. The total resistance of the device can now be described as a function of flow rate and throughput:

$$R_{\text{tot}}(J, \tilde{V}) = R_{\text{housing}}(J) + R_{\text{mem}}(\tilde{V}) \quad (14)$$

The calculation basis in Sect. 2.6 and 2.7 is summarized under the assumption that either the same process conditions are used in small scale and large scale, or the process-dependency of filter fouling is negligible.

2.6 Resistance-Based Scale-up Approach Applied to Constant Pressure Filtration

In this section, the calculation of the filtration curve for a large-scale device, based on a test filtration in small scale and water flow rate measurements in large scale and small scale is explained. As can be seen in Fig. 6e, resistances of a large-scale device (variables with index LS) and a small-scale device (variables with index SS) increase identically in

dependence of throughput in course of filtration. The following conclusion is obtained concerning the change of membrane resistance in course of filtration:

$$R_{\text{mem_LS}}^{\circ}(\tilde{V}) = R_{\text{mem_SS}}^{\circ}(\tilde{V}) \quad (15)$$

By transformation with Eq. (12), Eq. (16) is obtained:

$$R_{\text{mem_LS}}(\tilde{V})A_{\text{LS}} = R_{\text{mem_SS}}(\tilde{V})A_{\text{mem_SS}} \quad (16)$$

This equation can be used to calculate the membrane resistance of the large-scale device:

$$R_{\text{mem_LS}}(\tilde{V}) = R_{\text{mem_SS}}(\tilde{V}) \frac{A_{\text{mem_SS}}}{A_{\text{mem_LS}}} = \frac{R_{\text{mem_SS}}(\tilde{V})}{S} \quad (17)$$

The scale-up factor S is the relationship between the membrane areas of the small-scale and the large-scale device, in contrast to recent literature where the scale-up factor is usually related to batch size. The membrane areas A_{mem} are the effective membrane areas and can be determined by water flow rate measurements (Sect. 2.3).

$$S = \frac{A_{\text{mem_LS}}}{A_{\text{mem_SS}}} = \frac{R_{\text{mem_SS}}(\tilde{V})}{R_{\text{mem_LS}}(\tilde{V})} \quad (18)$$

In Eqs. (15)–(18), the specific resistance R° , resistance R , effective membrane area A_{mem} (Eq. (12)) and the scale-up factor S are used.

For scale-up, first the membrane resistance $R_{\text{mem_SS}}(\tilde{V})$ has to be calculated. For this Eq. (14) is used, with Eq. (13) for the housing resistance.

$$R_{\text{mem_SS}}(\tilde{V}) = R_{\text{tot_SS}}(\tilde{V}, J) - k_{\text{SS}}J_{\text{SS}} \quad (19)$$

By use of the scale-up factor S the membrane resistance $R_{\text{mem_LS}}$ and the respective filtration volume V_{LS} for the large-scale device is now calculated according to Eq. (20) and (21).

$$R_{\text{mem_LS}}(\tilde{V}) = \frac{R_{\text{mem_SS}}(\tilde{V})}{S} \quad (20)$$

$$V_{\text{LS}} = V_{\text{SS}}S \quad (21)$$

Afterwards the device resistance $R_{\text{tot_LS}}(\tilde{V}, J)$ of the large-scale device can be calculated using Eq. (6) (Darcy's law) and (14).

$$R_{\text{tot_LS}}(\tilde{V}, J) = R_{\text{housing_LS}}(J) + R_{\text{mem_LS}}(\tilde{V}) = \frac{\Delta p_{\text{tot}}}{\eta J_{\text{LS}}} \quad (22)$$

With regard to Eq. (13) for the housing resistance the following expression can be written:

$$k_{\text{LS}}J_{\text{LS}} + R_{\text{mem_LS}}(\tilde{V}) = \frac{\Delta p_{\text{tot}}}{\eta J_{\text{LS}}} \quad (23)$$

Flow rate J of the large-scale device can be calculated by transforming Eq. (23):

$$J_{\text{LS}}(\tilde{V}) = \frac{-R_{\text{mem_LS}}(\tilde{V}) + \sqrt{R_{\text{mem_LS}}^2(\tilde{V}) + 4k_{\text{LS}} \frac{\Delta p_{\text{tot}}}{\eta}}}{2k_{\text{LS}}} \quad (24)$$

The flow rate for the large-scale device can be calculated according to Eq. (24) after defining the viscosity η , the constant k_{LS} for the device and the process pressure Δp_{tot} . As a last step with the known datasets of flow rate and volume, the respective time dependency can be calculated:

$$t = \sum_{i=0}^t \Delta t_i = \sum_{i=0}^t \frac{\Delta V_i}{J_i} \quad (25)$$

With the calculated datasets of time, volume, flow rate and resistance the large-scale filtration curves can be plotted.

2.7 Resistance-Based Scale-Up Approach Applied to Constant Flow Rate Filtration

For constant flow rate filtration, scale-up is similar to constant pressure filtration in Sect. 2.6. First, according to Eq. (19), membrane resistance $R_{\text{mem_SS}}(\tilde{V})$ for the small-scale filtration has to be calculated. Afterwards, membrane resistance $R_{\text{mem_LS}}(\tilde{V})$ of the large-scale device has to be calculated according to Eq. (20). For the target flow rate, housing resistance is a constant (as J_{LS} is a constant) and just has to be added up according to Eq. (22) for calculation of the device resistance. Filtrate volume can be calculated by Eq. (21), the timescale is calculated by Eq. (25).

In constant flow filtration the filtration flow rate is in theory just a constant. So, the $J(\tilde{V})$ plot shows a straight line. However, in reality filtration flow rate is usually adjusted by a pump that generates pulsating pressure. In this case the fluctuations can be observed in the measured filtration flow rate. So, if the flow rate profile that is generated by the pump is known (because of old process data or because in the small-scale trial a comparable pump is used), this flow profile can be used for the calculation of the large-scale process data as well. This way the fluctuation of the pressure for the large-scale device can be predicted. This approach is used for the example given in Sect. 3.2.

The pressure difference across the large-scale device is received by transforming Eq. (23) to Eq. (26):

$$\Delta p(J, \tilde{V}) = k_{\text{LS}}J^2\eta + R_{\text{mem_LS}}(\tilde{V}) \quad (26)$$

With the generated datasets of time, volume, flow rate, resistance and differential pressure process now the large-scale filtration curves can be plotted.

3 Model Validation

In Sect. 2.6 and 2.7 it was shown that the filtration curve of a filter device can be calculated on the basis of the filtration curve of a scaling device and its resistance vs. throughput plot, $R_{\text{mem,SS}}(\tilde{V})$. Now two scaling examples are presented.

3.1 Upscaling Example – Constant Pressure Filtration

Small-scale filtration was performed at constant pressure filtration at 0.5 bar, using a 47-mm Sartopore[®] 2 membrane filter disc with 0.45 μm /0.2 μm nominal pore size combination. Large-scale filtration case is filtration through a size 4 capsule of Sartopore[®] 2 at 1 bar.

First, water flow rate has been measured at 0.3, 0.5 and 1 bar for both devices to determine the constant k_i and the initial membrane resistance $R_{\text{mem}}(\tilde{V} = 0)$ as described in Sect. 2.4. The measured resistance and water flow rate data of both devices are shown in Fig. 7 and Tab. 2.

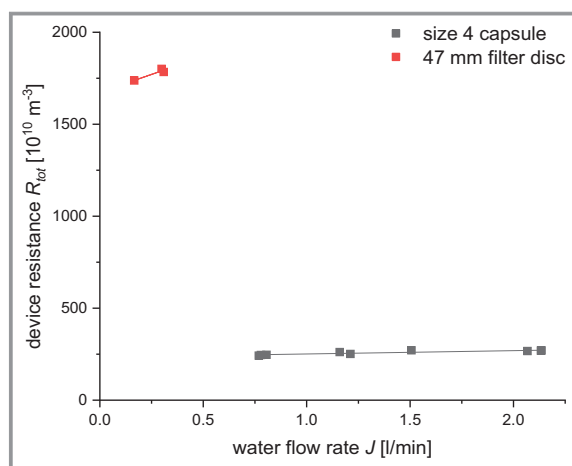


Figure 7. Results for water flow measurements of 47-mm filter disc and size 4 capsule of Sartopore[®] 2.

Table 2. Results of water flow rate measurements for 47-mm filter disc and size 4 capsule of Sartopore[®] 2.

Device	Slope k_i [$10^{13} \text{ min m}^{-6}$]	Intercept R_{mem} [10^{13} m^{-3}]	Effective membrane area A_{mem} [cm^2]
47 mm	390 ± 131	1.67 ± 0.03	14.1
Size 4 capsule	18 ± 3	0.233 ± 0.005	116
Scale-up factor		7.17	

The scale-up factor was calculated according to Eq. (18). With Eq. (18), the effective membrane area for the size 4 capsule of Sartopore[®] 2 can be calculated with

$A_{\text{LS}} = 116 \text{ cm}^2$. This value, which is used for the calculations, is lower than the embedded filter area of 150 cm^2 [13]. The difference between embedded and effective filter area can be explained by the different fluid dynamics of flat filter devices and pleated filter devices as already discussed in Sect. 2.4.

The device resistance is defined by the slope k_i and the membrane resistance $R_{\text{mem}}(\tilde{V} = 0)$. For the calculation of the membrane resistance $R_{\text{mem}}(\tilde{V})$ of the large-scale device Eq. (17) is used. Subsequently, Eq. (24) and (25) are used for calculation of filtration data for size 4 capsule. The resulting plots comparing the experimental and predicted values are depicted in Fig. 8, showing excellent agreement between both datasets.

3.2 Downscaling Example – Downscaling of a Constant Pressure Filtration Experiment to Constant Flow Filtration

With the approach presented in Sect. 2.7, constant flow filtration curves can be calculated based on a constant pressure filtration. In this section the procedure is demonstrated for a downscaling case. Large-scale filtration case is a constant pressure filtration at 0.5 bar using a 47-mm Sartopore[®] 2 membrane filter disc. Small-scale filtration case is filtration through a 25-mm Sartopore[®] 2 membrane filter disc at constant flow of $14 \text{ mL min}^{-1} \text{ cm}^{-2}$. Again, the particulate test solution described in Sect. 2.2 was filtered and the calculated data were finally verified by experiment.

As the membrane areas and the filtration flow rate are quite small, housing resistance in form of the constant k_i is assumed to be zero, as the standard deviations exceed the actual values for k_i . The effective membrane area is measured by the area of the filter disc that was colored brown by the test solution.

The results are shown in Fig. 9. First the volume is calculated by Eq. (21) (Fig. 9a). The timescale is received by Eq. (25). Eq. (26) is used for calculation of the differential pressure (Fig. 9d). By using Eq. (5), filtration flux data (Fig. 9b and 9e) is predicted.

No differences can be seen in plot (a) between predicted and experimental data, because this is the assumed dataset for the calculations of flux, differential pressure and resistance. Plot (b) and (e) show for the calculated flow rate data no straight line, because the values shown were calculated by derivation of the volume data obtained by constant pressure filtration. The important data for a process design is the pressure vs. time plot (d). Here it can be seen that the predicted data is at the beginning a little low and near the end too high compared to experiment. Possible explanations are due to a missing vent in the small-scale filter housing at the beginning of the experiment probably air at the pressure sensor increases the measurement values. The deviation at the end of the experiment could occur because of batch variations of the filter discs.

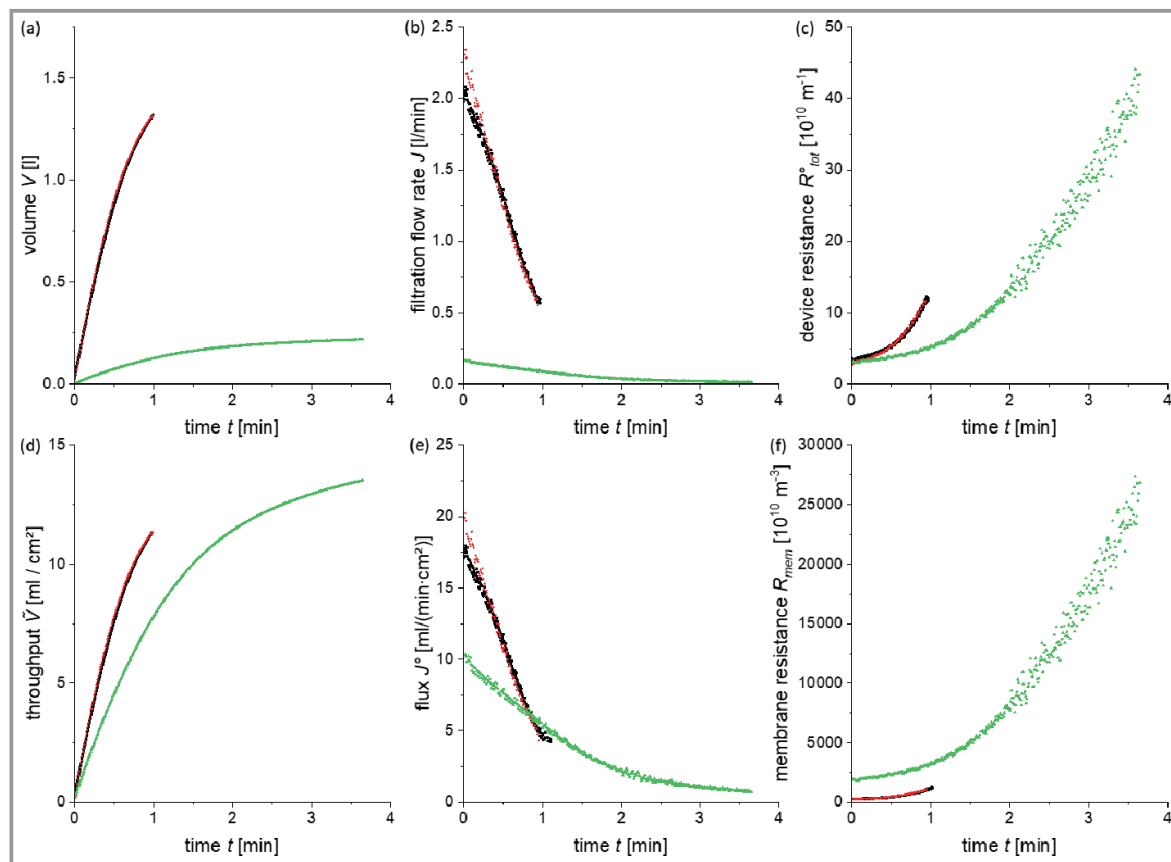


Figure 8. Filtration data of 14.1-cm² filter disc at 0.5 bar (green), size 4 capsule at 1 bar (red) and predicted data based on 47-mm filter disc for size 4 capsule at 1 bar (black).

4 Conclusions

In this work, a flow rate and resistance-based approach is presented for upscaling of filtration processes. For this concept, first the respective process conditions have to be defined (constant flow, constant pressure, batch size and maximum filtration time). Moreover, appropriate small-scale tests have to be performed.

The upscaling concept comprises:

- the measurement and analysis of filtration curves of a lab-scale filter device,
- the estimation of the required filter area and the selection of a suitable filtration device for filtration of a target filtration volume,
- the measurement of resistance and filter area of scaling and targeted filter device by pressure dependent H₂O-flow measurements,
- the modeling of the resistance vs. throughput plot (R_{tot} vs. \tilde{V}) of the targeted device under target filtration conditions; and finally flow rate and the filtered volume vs. time plots can be calculated.

Basic requirements for the calculations are the knowledge of the precise effective membrane areas and the device resis-

tances, both determined by water flow measurements. A resistance-in-series model is used to describe the device resistances.

The validity of this approach was demonstrated by filtration data of a particulate test solution through Sartopore[®] 2 membrane filters at different scale. An excellent comparability of predicted and experimental data could be achieved.

The necessary calculation approach is summarized. The modeling can be used for constant flow and constant pressure filtration and does not require the knowledge of the blocking mechanism. The approach can be used for upscaling and downscaling of a filtration process, which minimizes experimental efforts for process development.

Supporting Information

Supporting Information for this article can be found under DOI: <https://doi.org/10.1002/cite.201900025>.

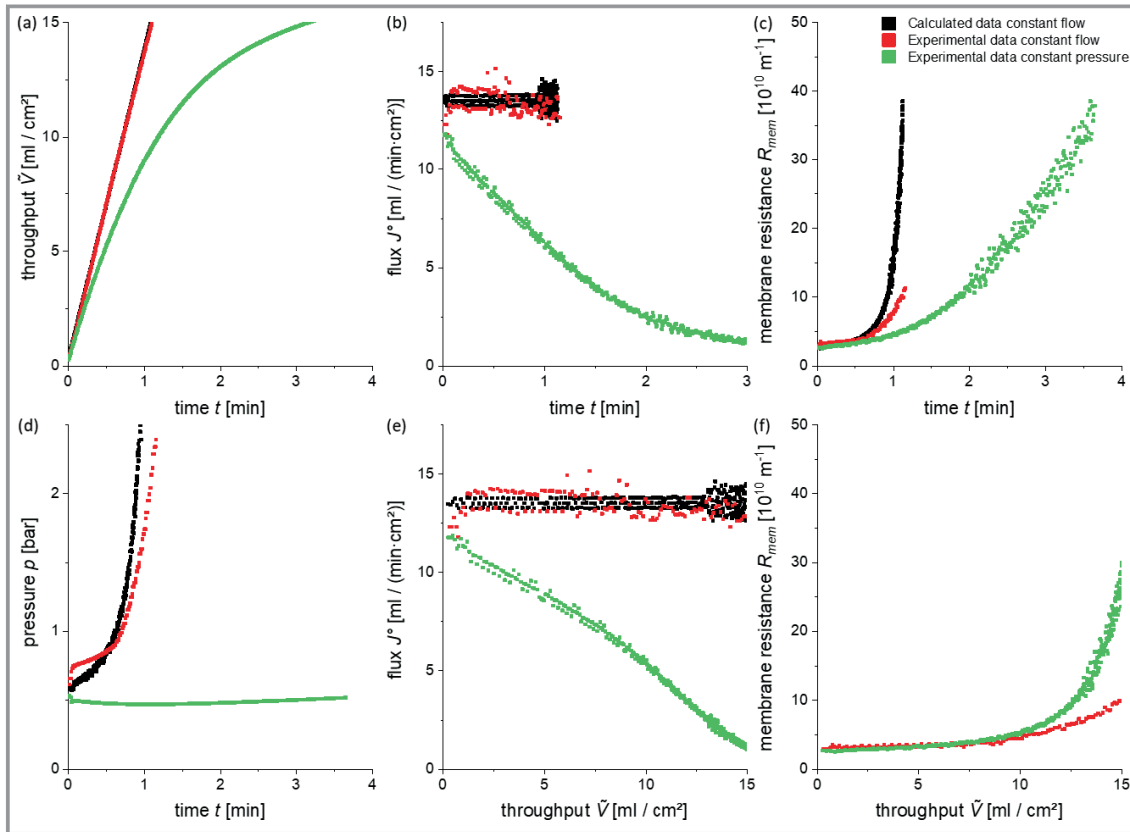


Figure 9. Prediction of a 25-mm constant flow filtration with $14 \text{ mL min}^{-1} \text{ cm}^{-2}$ out of a constant pressure filtration with a 47-mm filter disc at 0.5 bar pressure. The calculated data is compared to the experiment.

Symbols used

A_{mem}	$[\text{cm}^2]$	active membrane area	R_{in}	$[10^{10} \text{ m}^{-3}]$	resistance inlet
A_{batch}	$[\text{m}^2]$	area needed for filtration of a batch	R_{LS}	$[10^{10} \text{ m}^{-3}]$	membrane resistance large-scale device
A_{device}	$[\text{m}^2]$	membrane area within a device	R_{LS}°	$[10^{10} \text{ m}^{-1}]$	membrane resistance large-scale device
A_{SS}	$[\text{m}^2]$	membrane area used for small-scale experiments	R_{mem}	$[10^{10} \text{ m}^{-3}]$	membrane resistance
A_{LS}	$[\text{m}^2]$	membrane area used for large-scale experiments	R_{mem}°	$[10^{10} \text{ m}^{-1}]$	specific membrane resistance
A_{test}	$[\text{m}^2]$	filtration area used for test	R_{SS}	$[10^{10} \text{ m}^{-3}]$	membrane resistance of small-scale device
J	$[\text{mL min}^{-1}]$	flow rate	R_{SS}°	$[10^{10} \text{ m}^{-1}]$	membrane resistance small-scale device
J°	$[\text{mL min}^{-1} \text{ cm}^{-2}]$	filtration flux	R_{out}	$[10^{10} \text{ m}^{-3}]$	resistance outlet
k_i	$[10^{10} \text{ min m}^{-6}]$	constant, specific for each device and describes the relationship of device resistance and flow rate	R_{tot}	$[10^{10} \text{ m}^{-3}]$	measured resistance of a whole device
Δp	[bar]	pressure difference across membrane	R_{tot}°	$[10^{10} \text{ m}^{-1}]$	measured resistance of a whole device
Δp_{tot}	[bar]	pressure difference across device	S	[-]	scale-up factor
Re	[-]	Reynolds number	SF	[-]	safety factor for scale-up process design
R_{dev}°	$[10^{10} \text{ m}^{-1}]$	resistance of a device, normed by membrane area	t	[s]	time (progress of filtration experiment)
R_{housing}	$[10^{10} \text{ m}^{-3}]$	housing resistance	Δt	[s]	time difference between two adjacent data points

ΔV	[L]	difference in filtrate volume between two adjacent data points
V	[L]	filtrate volume
\tilde{V}	[L m ⁻²]	filtrate volume per effective membrane area
V_{Batch}	[L]	batch size of upscaled process
V_{LS}	[L]	filtrate volume as calculated out of small-scale experiment
V_{final}	[L]	maximum filterable amount determined by a test filtration
V_{SS}	[L]	filtrate volume as measured in small-scale experiment
η	[mPa s]	viscosity

References

- [1] Y. Lu, *Discov. Med.* **2002**, *1*, 8.
- [2] A. A. Shukla, J. Thömmes, *Trends Biotechnol.* **2010**, *28*, 253–261. DOI: <https://doi.org/10.1016/j.tibtech.2010.02.001>
- [3] D. Pedrites, C. Siletti, J. Jiménez, P. Psathas, Y. Mannion, *Pharm. Eng.* **2011**, *31*, 1–10.
- [4] D. Low, R. O'Leary, N. S. Pujar, *J. Chromatogr. B: Anal. Technol. Biomed. Life Sci.* **2007**, *848*, 48–63. DOI: <https://doi.org/10.1016/j.jchromb.2006.10.033>
- [5] *A-Mab: a Case Study in Process Development*, Version 2.1, CMC Biotech Working Group, **2009**.
- [6] A. S. Rathore, A. Shirke, *Prep. Biochem. Biotechnol.* **2011**, *41*, 398–421. DOI: <https://doi.org/10.1080/10826068.2011.613976>
- [7] H. F. Liu, J. Ma, C. Winter, R. Bayer, *MABs* **2010**, *2*, 480–499. DOI: <https://doi.org/10.4161/mabs.2.5.12645>
- [8] *Sterile Drug Products Produced by Aseptic Processing – Current Good Manufacturing Practice*, U.S. Department of Health and Human Services, Washington, DC **2004**.
- [9] R. van Reis, A. Zydney, *J. Membr. Sci.* **2007**, *297*, 16–50. DOI: <https://doi.org/10.1016/j.memsci.2007.02.045>
- [10] *Development and Manufacture of Protein Pharmaceuticals* (Eds: S. L. Nail, M. J. Akers), Springer US, Boston, MA, **2002**. DOI: <https://doi.org/10.1007/978-1-4615-0549-5>
- [11] S. Aldington, J. Bonnerjea, *J. Chromatogr. B: Anal. Technol. Biomed. Life Sci.* **2007**, *848*, 64–78. DOI: <https://doi.org/10.1016/j.jchromb.2006.11.032>
- [12] J. L. Novais, M. Hoare, *Biotechnol. Bioeng.* **2001**, *75*, 143–153. DOI: <https://doi.org/10.1002/bit.1182>
- [13] *Product Information SPK2167-e1*, Sartorius Stedim Biotech GmbH, Göttingen **2017**.
- [14] *Filtration and Purification in the Biopharmaceutical Industry* (Eds: T. H. Meltzer, Maik W. Jorntz), Drugs and the Pharmaceutical Sciences, Vol. 174, CRC Press, Boca Raton, FL **2008**.
- [15] M. C. Manning, D. K. Chou, B. M. Murphy, R. W. Payne, D. S. Katayama, *Pharm. Res.* **2010**, *27*, 544–575. DOI: <https://doi.org/10.1007/s11095-009-0045-6>
- [16] S. R. McGuffee, A. H. Elcock, *J. Am. Chem. Soc.* **2006**, *128*, 12098–12110. DOI: <https://doi.org/10.1021/ja0614058>
- [17] A. M. Allmendinger, *Rheological investigation of manufacturability and injectability of highly concentrated monoclonal antibody formulations*, Ph.D. Thesis, Universität Basel **2014**.
- [18] E. Rosenberg, *Aggregation of Therapeutic Antibodies in the Course of Downstream Processing*, Ph.D. Thesis, Ludwig-Maximilians-Universität München **2010**.
- [19] S. Uchiyama, *Biochim. Biophys. Acta* **2014**, *1844*, 2041–2052. DOI: <https://doi.org/10.1016/j.bbapap.2014.07.016>
- [20] C. A. Challener, *BioPharm. Int.* **2015**, *28*, 26–28.
- [21] S. Giglia, G. Straeffer, *J. Membr. Sci.* **2012**, *417–418*, 144–153. DOI: <https://doi.org/10.1016/j.memsci.2012.06.026>
- [22] C. C. Ho, A. L. Zydney, *J. Membr. Sci.* **2002**, *209*, 363–377. DOI: [https://doi.org/10.1016/S0376-7388\(02\)00282-X](https://doi.org/10.1016/S0376-7388(02)00282-X)
- [23] D. M. Kanani, X. Sun, R. Ghosh, *J. Membr. Sci.* **2008**, *315*, 1–10. DOI: <https://doi.org/10.1016/j.memsci.2008.01.053>
- [24] M. E. Laska, R. P. Brooks, M. Gayton, N. S. Pujar, *Biotechnol. Bioeng.* **2005**, *92*, 308–320. DOI: <https://doi.org/10.1002/bit.20587>
- [25] L. McBurnie, B. Bardo, *Pharm. Technol.* **2004**, 13–23.
- [26] B. S. Chang, B. Yeung, in *Formulation and Process Development Strategies for Manufacturing Biopharmaceuticals* (Eds: F. Jameel, S. Hershenson), John Wiley and Sons, Hoboken, NJ **2010**, 69–104. DOI: <https://doi.org/10.1002/9780470595886.ch3>
- [27] A. Belgaid, B. Benaji, N. Aadil, S. Moussamih, Y. Khayati, S. Taouadi Benchekroune, M. El Guezzar, *J. Chem. Pharm. Res.* **2014**, *6*, 760–770.
- [28] *Vmax™ Constant Pressure Test*, Protocol PR1326EN00 Rev A, EMD Millipore Corporation, Burlington, MA **2014**.
- [29] *Product Information SPK2145-e1*, Sartorius Stedim Biotech GmbH, Göttingen **2016**.
- [30] www.pall.de/main/biopharmaceuticals/product.page?lid=gri78lfw (accessed on December 19, 2018).
- [31] <https://de.slideshare.net/MilliporeSigma/scaleup-of-high-area-filters-for-microfiltration-of-biological-fluids-points-to-consider-for-reliable-scaleup> (accessed on May 23, 2019).
- [32] P. Rajniak, S. C. Tsinontides, D. Pham, W. A. Hunke, S. D. Reynolds, R. T. Chern, *J. Membr. Sci.* **2008**, *325*, 223–237. DOI: <https://doi.org/10.1016/j.memsci.2008.07.049>
- [33] H. Lutz, *J. Membr. Sci.* **2009**, *341*, 268–278. DOI: <https://doi.org/10.1016/j.memsci.2009.06.015>
- [34] S. Giglia, K. Rautio, G. Kazan, K. Backes, M. Blanchard, J. Caulmare, *J. Membr. Sci.* **2010**, *365*, 347–355. DOI: <https://doi.org/10.1016/j.memsci.2010.09.032>
- [35] A. Kumar, J. Martin, R. Kuriyel, *PDA J. Pharm. Sci. Technol.* **2015**, *69*, 74–87. DOI: <https://doi.org/10.5731/pdajpst.2015.01006>
- [36] E. Iritani, N. Katagiri, *KONA Powder Part. J.* **2016**, *33*, 179–202. DOI: <https://doi.org/10.14356/kona.2016024>
- [37] A. Saluja, D. S. Kalonia, *Int. J. Pharm.* **2008**, *358*, 1–15. DOI: <https://doi.org/10.1016/j.ijpharm.2008.03.041>
- [38] S. Giglia, D. Yavorsky, *PDA J. Pharm. Sci. Technol.* **2007**, *61*, 314–323.
- [39] G. Bolton, D. LaCasse, R. Kuriyel, *J. Membr. Sci.* **2006**, *277*, 75–84. DOI: <https://doi.org/10.1016/j.memsci.2004.12.053>
- [40] C. C. Ho, A. L. Zydney, *J. Colloid Interface Sci.* **2000**, *232*, 389–399. DOI: <https://doi.org/10.1006/jcis.2000.7231>
- [41] S. Giglia, G. Straeffer, *Bioprocess. J.* **2013**, *12*, 31–39. DOI: <https://doi.org/10.12665/J123.Giglia>
- [42] M. Discacciati, A. Quarteroni, *Rev. Mat. Complutense* **2009**, *22*, 315–426.
- [43] *VDI-Wärmeatlas*, Springer-Verlag, Berlin **2006**.
- [44] A. Piry, A. Heino, W. Kühnl, T. Grein, S. Ripberger, U. Kulozik, *J. Dairy Sci.* **2012**, *95*, 1590–1602. DOI: <https://doi.org/10.3168/jds.2011-4292>
- [45] Z. Li, A. H-Kittikun, W. Youravong, *Biochem. Eng. J.* **2008**, *38*, 226–233. DOI: <https://doi.org/10.1016/j.bej.2007.07.005>
- [46] *Sartopore® 2 γ -Irradiatable or Autoclavable T-Style MaxiCaps® 0.1 & 0.2 μm* , Validation Guide SPK5784-e1, Sartorius Stedim Biotech GmbH, Göttingen **2013**.